Multiscale-multifluid simulations of the 26 February 2008 substorm: Evidence for internal triggering of a substorm

E. M. Harnett,[1] R. M. Winglee,[1] and T. Lerud[1]

[1] Multiscale-multifluid simulations are used to provide high-resolution (~470 km) simulations of the 26 February 2008 substorm that was well observed by the THEMIS spacecraft to investigate whether the substorm was internally or externally triggered. This substorm occurred during an extended (1 h 45 min) period of weak (−2.5 to −1.5 nT) southward interplanetary magnetic field (IMF). Simulation results show that this substorm was internally triggered well before the IMF start to become more northerly. The southward IMF leads to an enhancement in the cross-polar cap potential, strong thinning of the current sheet, and pseudo-breakup in association with patchy reconnection. The southward IMF also produces an enhancement in the outflow of ionospheric oxygen into the current sheet. Because of the tilt of the magnetic field the strongest outflows originate from the southern polar cap. The arrival of these heavy ions in the tail occurs about 10 min prior to the observed substorm onset and leads to enhanced tail reconnection, including flux rope development and fast earthward flows. The interaction of these fast flows at the inner edge of the plasma sheet is closely associated with auroral onset, indicating that the substorm is internally triggered. Comparison with THEMIS data suggests that reconnection occurred earlier than THEMIS observations. The results show onset is associated with processes at the inner edge of the plasma sheet and is not directly related to the onset of reconnection. Comparison with THEMIS data indicates that processes at scale lengths less than 500 km are occurring.

1. Introduction

[2] On 26 February 2008, the THEMIS spacecraft were fortuitously positioned in the magnetotail to observe reconnection occurring prior to substorm onset [*Angelopoulos et al.*, 2008]. Reconnection events were seen at the P1 and P2 spacecraft at approximately 20 R_E at 0450:28 UT and 0450:38 UT, respectively, while auroral intensification was seen at 0451:39 UT and high-latitude Pi2 onset at 0452:00 UT and substorm expansions phase at 0452:21 UT. Because the reconnection signatures were observed at least 2 min prior to substorm onset it was concluded that the substorm was initiated by tail reconnection.

[3] Substorm timing is an issue that is still being debated. Some observations, such as those by *Baker et al.* [2002], suggest that onset occurs several minutes after reconnection occurs. *Baker et al.* [2002] correlated information from several geostationary spacecraft and Cluster, with global auroral images from IMAGE and determined auroral onset occurred 7 min after signatures of reconnection were detected by Cluster. In this case, the Cluster satellites were ~19 R_E down tail. Other observations suggest that onset occurs within a minute or two of reconnection. For example *Meng and Liou* [2004] conducted a statistical study of Polar and Geotail data and found a mean time delay of 2–3 min from the observation of fast flows (many times used as a proxy for a signature of reconnection) in the tail and auroral breakup.

[4] Also debated is the location of the plasma dynamics which lead to substorm onset, with the current disruption (CD) model [*Lui et al.*, 1992; *Lui*, 1996] stating that processes near ~10 R_E lead to substorm onset while the near-Earth neutral line (NENL) model [*Hones*, 1984; *Baker et al.*, 1996] indicates that reconnection at ~20 R_E leads to substorm onset. The 26 February 2008 storm is no less controversial with *Lui et al.* [2009] arguing that auroral zone current structures become enhanced before reconnection is observed by the THEMIS satellites and therefore the reconnection is unrelated to substorm onset, while *Angelopoulos et al.* [2009] argue that many other parameters must also be considered when determining substorm onset.

[5] Previous multifluid-multiscale simulations of an internally triggered substorm for an idealized case [*Winglee et al.*, 2009] were used to investigate the validity of the CD model verses the NENL model for describing the events preceding substorm onset. The high spatial and temporal resolution of the simulations lead to the first model results to

[1]Department of Earth and Space Sciences, University of Washington, Seattle, Washington, USA.
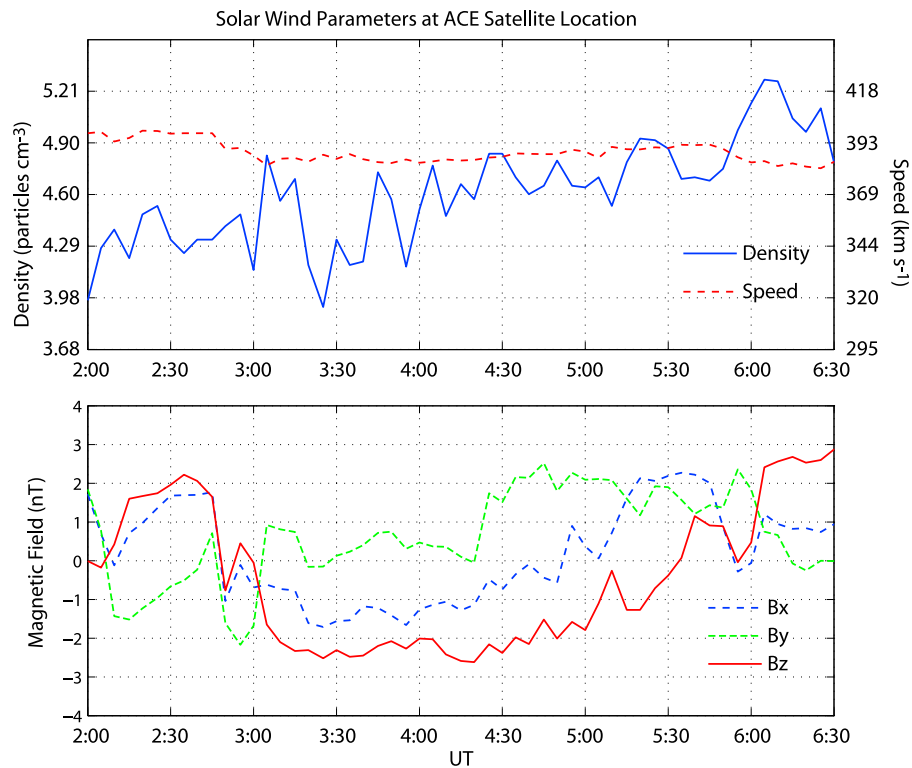
Figure 1. The solar wind conditions as measured by the ACE spacecraft. Data courtesy CDAWeb.

show earthward traveling flux ropes occurring in equal frequency as tailward traveling flux ropes in the postplasmoid current sheet, in agreement with Cluster observations [*Slavin et al.*, 2003]. The simulation results showed that the formation of an X line and plasmoid ejection are only precursors to substorm onset. Instead, earthward traveling flux ropes, formed through Y line reconnection, inject plasma into the inner edge of the plasma sheet. These injections can lead to either pseudo-breakup events or substorm onset, depending on the size and intensity of the flux ropes. The timing between the Y line reconnection that generated the flux ropes and the injection of plasma into the ionosphere along the field lines at the inner edge of the plasma sheet was on the order of 1 min.

[6] In this paper we present results from multiscale-multifluid simulations of the 26 February 2008 substorm. Data from synthetic spacecraft within the simulation are compared to the THEMIS observations by *Angelopoulos et al.* [2008] in order to validate the simulation results. Data from other locations within the simulation are also presented in order to put the local observations at satellite locations within a global context, establishing both timing and cause of substorm onset. Timing of observations of reconnection within the model is compared to observations of reconnection by THEMIS in order to investigate the roll of reconnection in substorm onset.

2. Model

[7] The simulations presented in this paper use the multifluid technique [*Winglee*, 2004] but also utilize a refined gridding technique to yield local grid resolutions of 470 km in the magnetotail of a global multifluid simulation. This is accomplished by first establishing a global equilibrium at coarse (0.3 R_E) resolution for nonsubstorm/nonstorm conditions. The system is then driven by the desired solar wind conditions. At key times the refined gridding system is initiated around the region of interest to desired resolution. Plasma and field quantities are passed between grid systems at each time step ensuring full coupling between the grid systems. This makes the code not only multifluid but also multiscale and allows us to investigate the roles of plasma beta and external forcing on the evolution of the current sheet/reconnection region within the global context.

[8] The results shown are in the GSM coordinate system, with the x axis parallel to the solar wind, pointing toward the Sun, z is perpendicular to the ecliptic planet, pointing in the northerly direction and y completes the system pointing opposite to the direction of orbital motion. For these results a region of 0.074 R_E (470 km) resolution is included in the tail between −8.85 R_E and −25.5 R_E along x, 8.85 R_E and 0 R_E along y, −5.02 R_E and 0 R_E along z, thus ensuring that the reconnection region is resolved. The resolution of the grid increases further out from the central tail is equal to 0.295 R_E around the Earth, increasing to 2.4 R_E far down tail and in the solar wind. A detailed description of the equations solved can be found by *Winglee et al.* [2009].

[9] The simulations incorporate four fluids: one electron fluid, and the solar wind H^+, ionospheric H^+, and ionospheric O^+ ion components. The model was driven with the solar wind conditions, as measured by ACE and shown in Figure 1. The earth's dipole is tilted 19° off the normal to
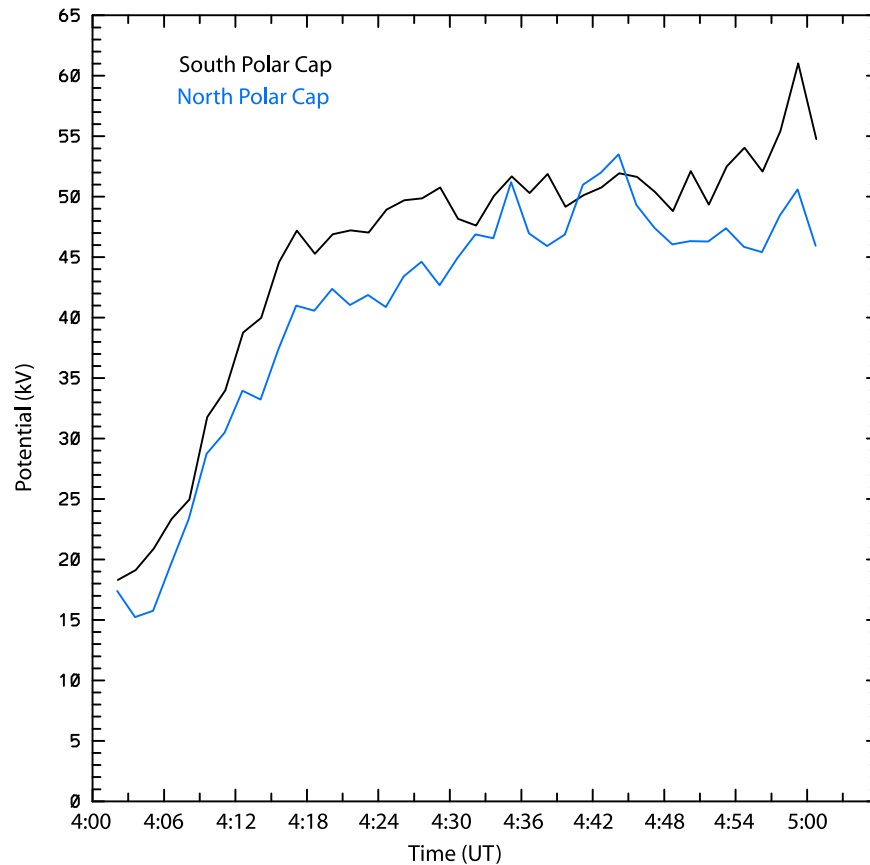
Figure 2. The time evolution of the cross-polar cap potential as determined within the simulations.

the ecliptic plane and held constant at this angle throughout the time period shown in this paper.

3. Results

3.1. Global View

[10] Figure 2 shows the development of the cross-polar cap potential. There is approximately a 1 h propagation time from when the southward IMF is observed by ACE to its arrival at the magnetosphere. This southward IMF leads in an increase in the cross-polar cap potential starting shortly after 0400 UT. The potential rises rapidly in a 15 min period to reach a value of about 45 kV for the summer (southern) hemisphere with the potential in the winter (northern) hemisphere being about 10% smaller at 40 kV. After this rapid rise there is a slow increase in the potential to about 50 kV with the northern hemispheric potential reaching the same value as the southern hemisphere at 0442 UT or about 10 min prior to the observed substorm onset time. Thus, the cross-polar cap potential responds to a near-saturated level during the growth phase but a specific trigger for onset is not seen in its temporal behavior.

[11] The corresponding development of the auroral currents in the northern hemisphere is shown in Figure 3. The current structure at 0401 UT (Figure 3a) represents the quiescent current structure. *Pu et al.* [2010] identify a substorm occurring at 0405 UT, but with a peak AE of ~80, the auroral zone intensification is much smaller than the sub-

storm at 0451, with a peak AE of ~200. Small variations in the auroral current structure are seen in the model around 0400 UT but are not shown as they are on a much smaller scale than the intensification around 0450 UT, which is the focus of this paper.

[12] The nightside currents first begin to intensify around 0430 UT, peaking at 0436 UT, and then begin dissipating around 0440 UT (Figures 3c–3e). This intensification is associated with pseudo-break up. At 0451 UT (Figure 3i), the currents intensify again and the peak current begins moving poleward near local midnight while the current oval expands. Substorm onset is identified as occurring at 0451 UT, the same time identified by the THEMIS team from auroral intensification [*Angelopoulos et al.*, 2008], through this intensification of the currents and movement of the peak current. The auroral currents are also seen to increase and expand to lower latitudes in conjunction with the growth phase. However, these current are primarily strongest in the dawn and dusk sector with little current in the midnight sector. The substorm lasts for approximately 40 min. Thus, the model is able to identify auroral onset (as well pseudo-breakup) within the context of the field-aligned currents. The issue is then what are the circumstances and processes that drive onset.

[13] Figure 4 shows contour plots of B_z in the equatorial plane, the noon-midnight meridian and across the midtail at $x \sim -40$ R_E. The areas of negative B_z in the equatorial plane provide an indicator of when and where reconnection is
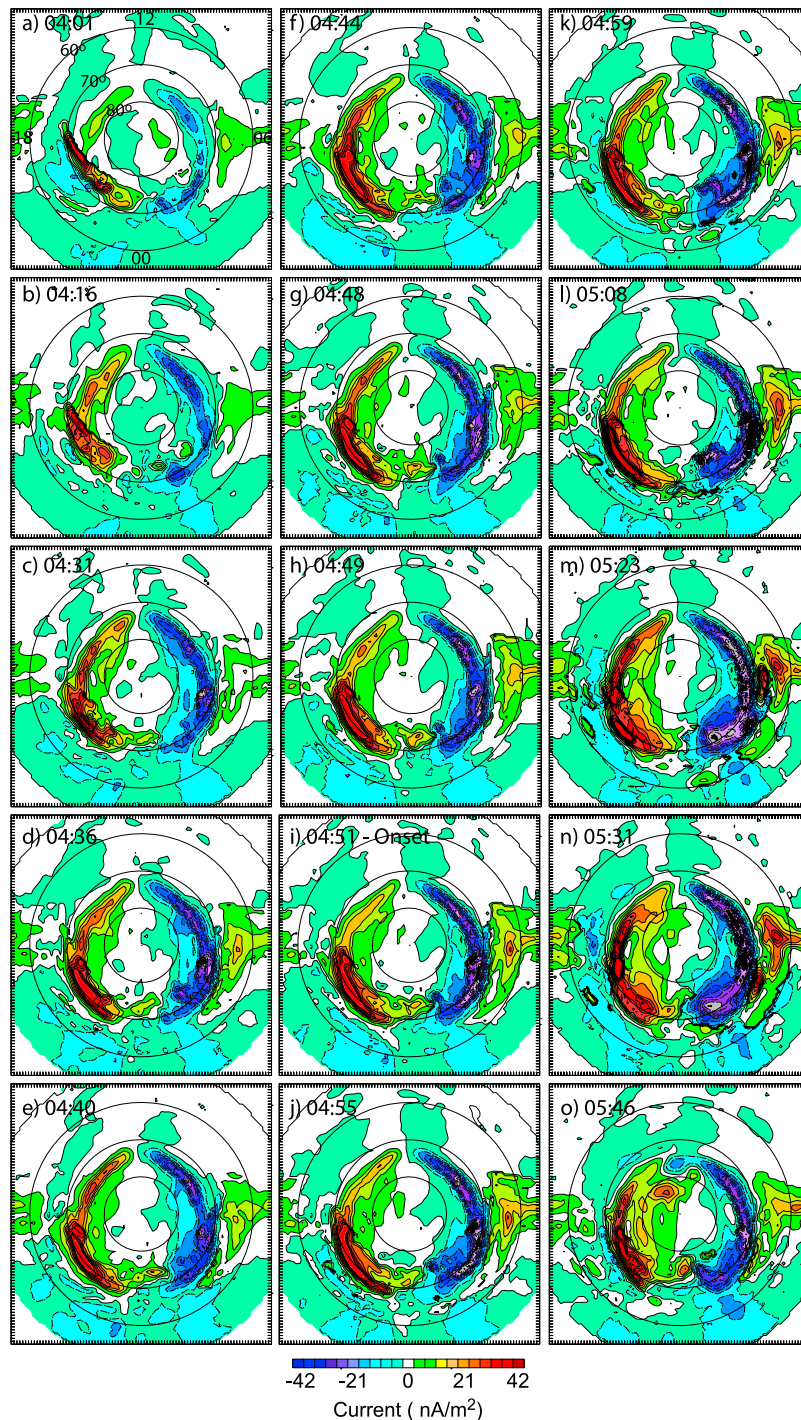
Figure 3. The time evolution of the currents in the auroral oval as determined by the simulation. The currents are determined from the model just above the inner boundary, at 2.5 R_E, and then mapped down to what would be observed at 100 km. The mapping of the current assumes that total current is conserved. The area of the current regions is mapped along dipole-like field lines assuming the area goes as r^3.

occurring in the tail. Patchy reconnection is seen to start to occur at around 0419 UT and this corresponds to the time when the rate of increase in the cross-polar potential sharply declines. This patchy reconnection continues to slowly grow until 0447 UT, when there is reconnection across the bulk of the tail at x ~ 20 R_E. The development of this larger reconnection region is consistent with the findings of

Angelopoulos et al. [2008] as they infer reconnection starting at 0450 UT. However, the model results indicate that smaller scale reconnection is occurring as much as 30 min earlier than the onset of this larger-scale reconnection. In other words, while tail reconnection may be necessary for onset, it is not sufficient.
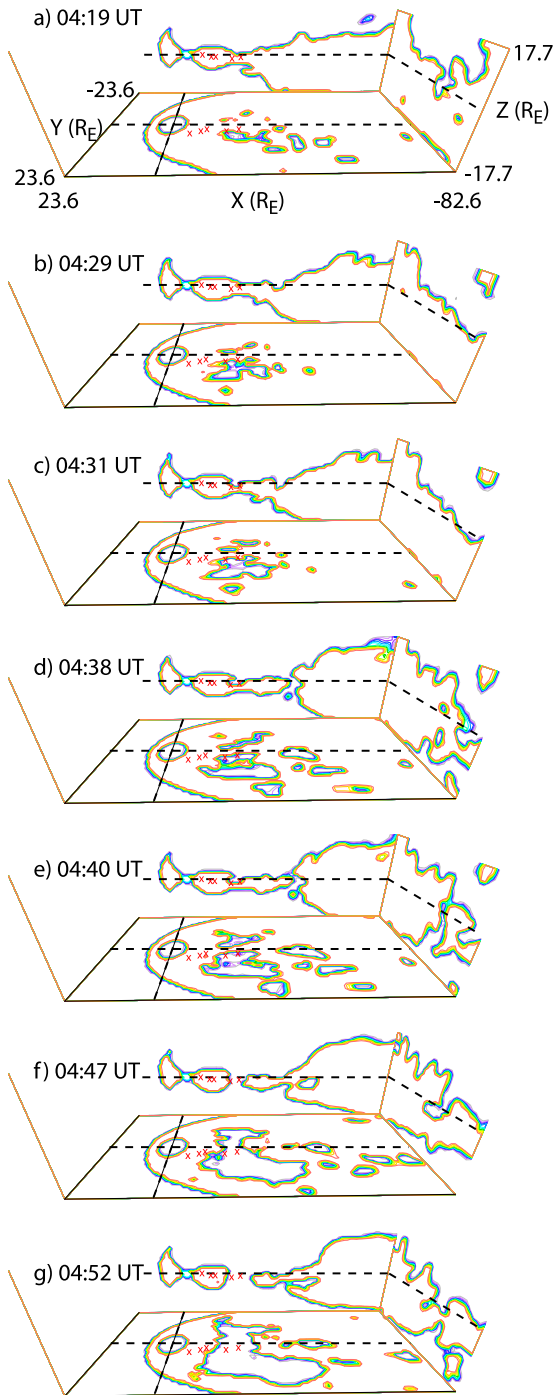
Figure 4. The time evolution of reconnection in the magnetotail, as indicated by B_z component in saturation. Reconnection is indicated by location of large gradients (i.e., color change). The 2-D cuts are through $z = 0$ (bottom panel), $y = 0$ (back panel), and $x \sim -40 R_E$ (right panel). An animation of the plots between 0402 and 0501 UT is provided (see Animation 1). The dotted lines indicate the noon-midnight meridian and dawn-dusk terminator in the bottom panels and the $z = 0$ axis in the back and right panels. The red Xs indicate, in projection, the approximate average location of the THEMIS satellites.

[14] It is also important to note that this onset occurs during a period when the IMF is still southward and prior to the northward turning in the IMF occurs. This suggests that the triggering of the substorm, from both model and observational viewpoints, is that of an internal trigger as opposed to an external trigger.

[15] In order to better understand the relationship between reconnection and substorm onset, Figure 5 shows the time evolution of the electron pressure and relative oxygen concentration in the noon-midnight meridian. The positions of the THEMIS spacecraft are shown by the dots on the electron pressure contours. The plasma pressure gives an overall indicator of the structure of the plasma sheet, with the pressure contours approximately following the field lines. The low-pressure regions (blue) indicative of the lobe, the yellow regions on the nightside indicate the plasma sheet, and the sheath is indicated by the brown/red regions on the dayside. The derived configuration is very close to the schematic developed by *Angelopoulos et al.* [2008] to describe the THEMIS observations.

[16] The model results show that the thinning of the current sheet is initiated at the beginning of the growth phase, as seen by the reduction in the width of the tail plasma pressure. This thinning is emphasized by the white contour lines from the electron pressure which are for the same fixed pressure within each of the panels. A Y line configuration is seen to develop at 0431 UT (as indicated by the white contour line). The Y line is seen to grow in length down the tail until between 0446 and 0453 UT. The formation of the line occurs well before onset is observed [cf. *Winglee et al.*, 2009]. Between 0446 and 0453 UT, there is dipolarization of the plasma and magnetic field. Dipolarization is consistent with the intensification of the auroral currents in association with substorm onset.

[17] The pressure contours are overlaid on the relative O^+ density on the right hand side of Figure 5 so that the position of the ionospheric outflows relative to the current sheet can be determined. It is seen that the relative concentration of O^+ in the plasma sheet is initially very low at less than ~1%. With the increase in cross-polar cap potential, the flow of oxygen ions into the tail current sheet is enhanced, particularly in the southern hemisphere. The total density of ionospheric ions does not increase substantially, rather the percentage of oxygen ions increases. In fact, the density of ionospheric hydrogen flowing out of the southern polar cap decreases during this time period (Figure 6). These oxygen-enhanced flows reach the Y line at 0438 UT, i.e., about 10–14 min prior to onset but at the time when an expansion of the tail reconnection region occurs. Feeding of enhanced oxygen fluxes into the Y line through the last frame that is shown, occurs past onset. The arrival of O^+ in the tail after the initiation of tail reconnection but before onset suggests that it has the potential to participate in the triggering of substorm onset. In the following we investigate how the model signatures relate to the THEMIS observations.

3.2. Comparison to THEMIS Data

[18] Plasma and field values at the location of the THEMIS satellites were recorded during the simulation for comparison to actual THEMIS data. For the results presented in this paper, the satellites will be named according to the nomenclature established by *Angelopoulos et al.* [2008].
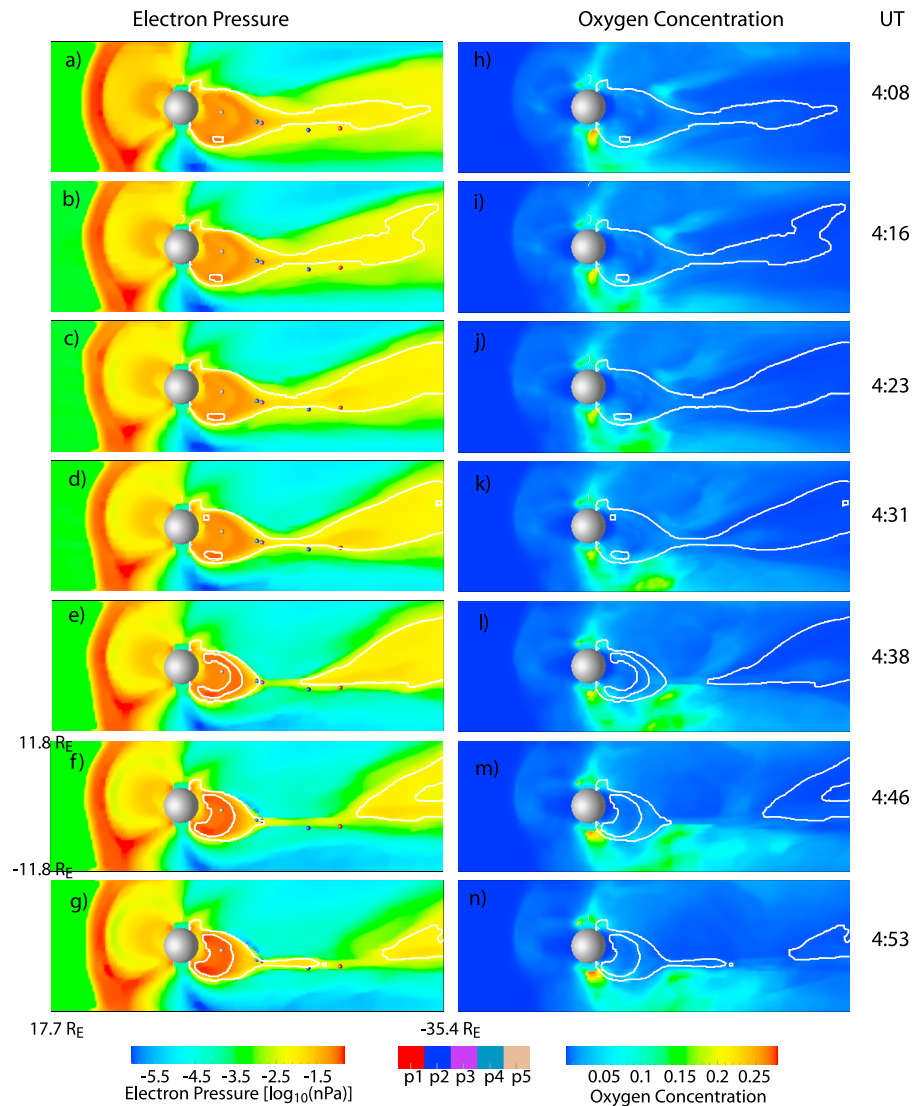
Figure 5. The time evolution of the electron pressure and the ionospheric oxygen concentration in the noon-midnight meridian. A white contour line indicates a value of −2.2 (outer contour) and −1.0 (inner contour) on the electron pressure plot at each time. The contour line is replicated at the same location on the concentration plots. Oxygen concentration is defined as the ionospheric oxygen number density divided by the total ion number density (ionospheric oxygen + ionospheric hydrogen + solar wind hydrogen). The average locations of the THEMIS satellites are also shown in the electron pressure plots.

The satellites within the simulation moved along a track similar to the actual satellite trajectory. To account for uncertainty within the simulations, at every point along the trajectory, the location of the synthetic satellite within the simulation was shifted by the amount listed in Table 1. As will be shown, just a small offset in the observing location relative to the inner edge of the plasma sheet and reconnection region can significantly change the results.

[19] Figures 7, 8 and 9 show the magnetic field and velocity components at both the actual and simulation spacecraft. Figures 10, 11, and 12 show the ion energy spectrograms at both the actual and simulation spacecraft. While data was sampled in the simulations at all five spacecraft locations, only data from P1, P3, and P5 are shown for brevity. These spacecraft represent observations

from three distinct locations. P1 was inferred to have been tailward of the reconnection region. P2–P4 were earthward of the inferred reconnection location and all within the plasma sheet. Of these three spacecraft P3 was selected as it was in between P2 and P4. P5 was in the plasmasphere.

[20] Reconnection was inferred to have occurred between the P1 and P2 satellites with the first evidence arriving at the P1 satellite at 0450 UT in the form of a tailward flow and a southward and duskward turning of the magnetic field [*Angelopoulos et al.*, 2008]. The simulation results shows a similar tailward flow of first the ionospheric hydrogen and then the oxygen (Figures 7d and 7e). At the same time, the B_z component of the magnetic field turns southward (Figure 7b) and the mean energy of the ionospheric hydrogen increases from 200 eV to 1 keV (Figure 11d).
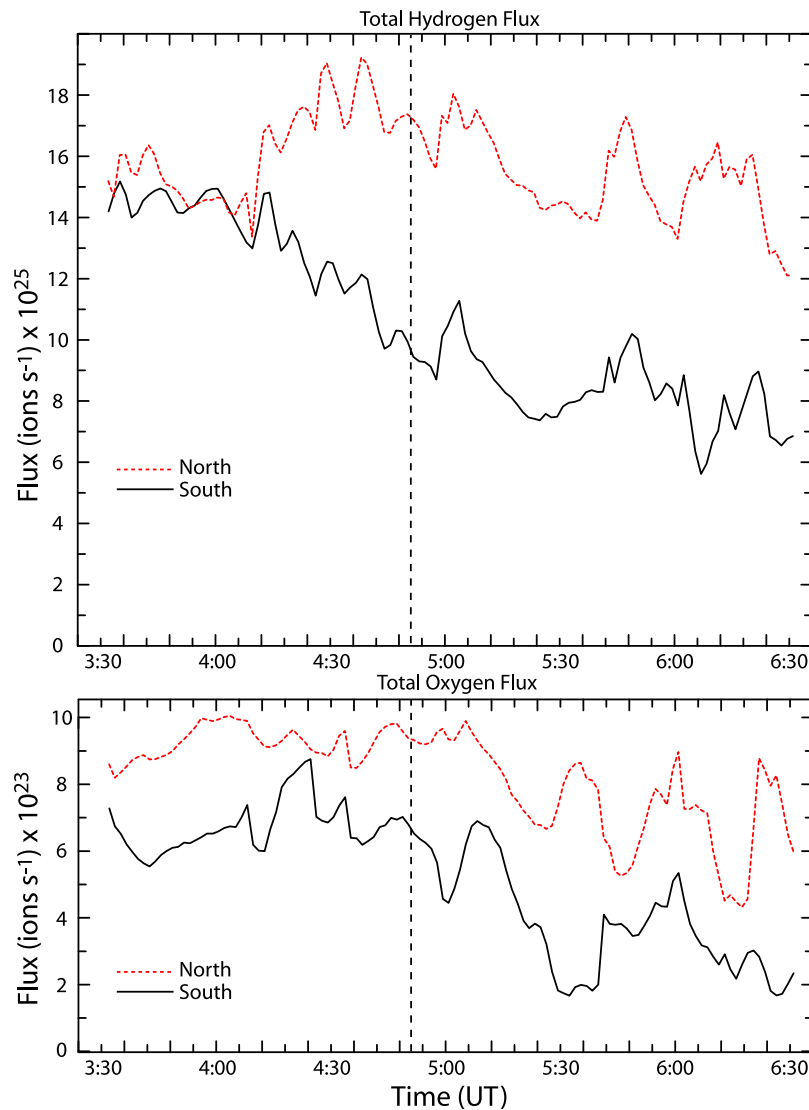
Figure 6. The rate of ionospheric outflows out of the polar cap as determined within the simulations for both poles. (top) Hydrogen. (bottom) Oxygen.

[21] After the initial tailward flow, the P1 spacecraft saw an earthward flow (Figure 7c). The simulation spacecraft also observed a high-speed flow at the same time but in the tailward direction. Figures 13 and 14 show the magnetic field configuration and 3D surfaces of earthward and tailward flows as well as the location of the five spacecraft. Figure 14 shows the same quantities as Figure 13 but at higher spatial and temporal resolution, as well as from a different view. The initial tailward flow can be seen in Figures 13c and 14f–14j. For the subsequent earthward flow, Figures 14m and 14n indicate that while the P1 spacecraft (its location highlighted by the red arrow) in the simulation is embedded in a tailward (pink) flow, a large earthward (blue) flow is present just duskward of the spacecraft. Flux ropes are present at various times, such as the center of Figures 14a–14b, upper right corner of Figures 14c and 14f, and the right edge of the Figure 14h. The important point though is that there are substantial variations occurring in the tail dynamics and changing the

observing position by just a few hundred km can dramatically change the results.

[22] Comparison of the oxygen velocity (Figure 7e) with the periodic signal in the spectrograms (Figure 11) indicates that the periodicity is on time scale of oxygen cyclotron

Table 1. The Offsets From the Average Locations of the Actual Satellites Given by *Angelopoulos et al.* [2008], Given in R_E with Directions in GSM Coordinates[a]

Satellite	X	Y	Z
THEMIS-A (P5)	−0.10	0.0	−0.5
THEMIS-B (P1)	−0.25	0.25	0.0
THEMIS-C (P2)	0.25	0.25	0.0
THEMIS-D (P3)	1.0	0.0	0.25
THEMIS-E (P4)	1.0	0.0	0.10

[a]The satellite nomenclature, as defined by *Angelopoulos et al.* [2008], is given in parentheses in the first column and will be used throughout the paper.
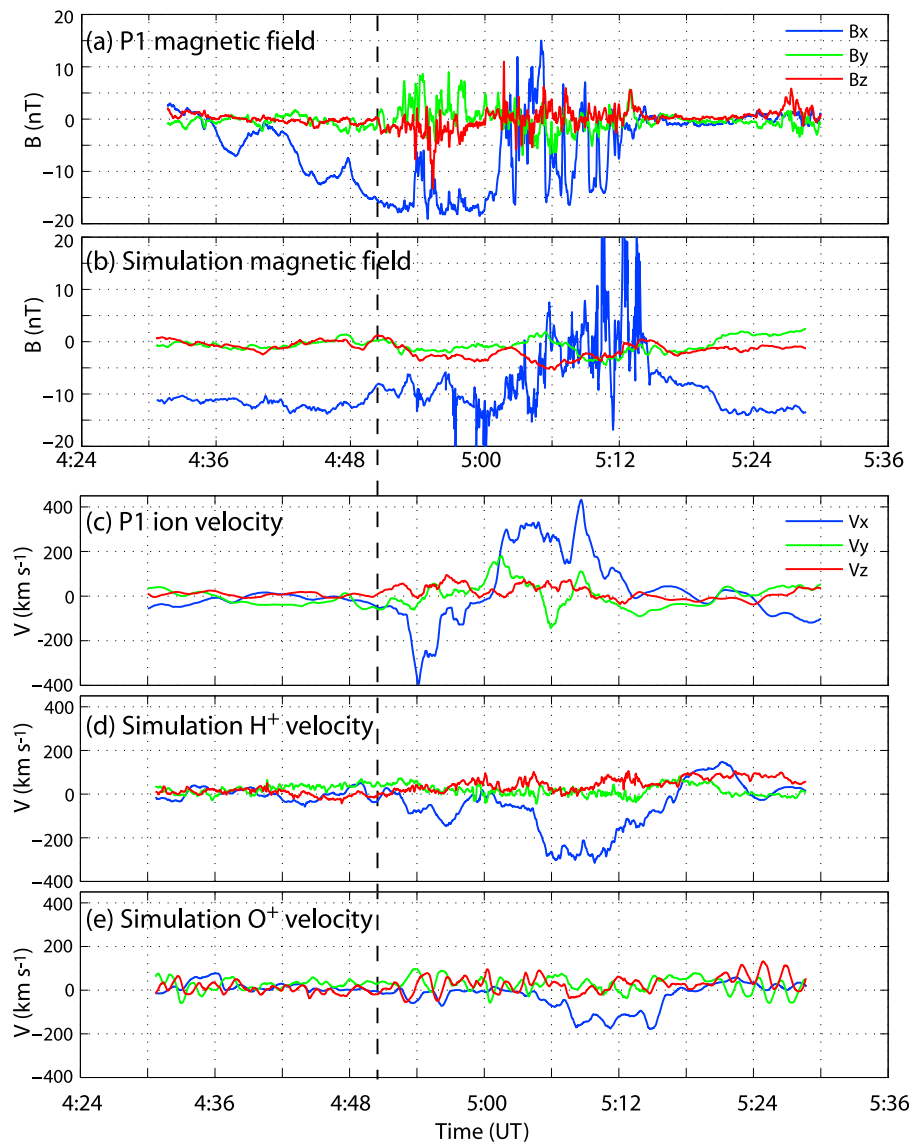
Figure 7. Magnetic field and velocity components for the P1 satellite. (a) Observed values. (b) Magnetic field from the simulations. (c) Observed plasma velocity components. (d and e) Velocity components for the ionospheric H$^+$ and O$^+$, respectively, from the simulations. The THEMIS satellites do not distinguish ion species. The dotted vertical line is the time identified by *Angelopoulos et al.* [2008] that the P1 satellite saw evidence of reconnection effects (~0450:38 UT).

frequency. As the periodicity is present in both the oxygen and hydrogen spectrograms (Figures 11c and 11d), this indicates that, even though the relative density of oxygen is a few percent, oxygen plays a central role in the dynamics of the plasma sheet during active periods. The simulation spectra also suggest that some of the increase in flux observed by the actual spacecraft post-reconnection is due to an increase in oxygen flux.

[23] For the P3 spacecraft, the simulation initially do not appear to agree with actual observations as well as at the P1 location just discussed. This is most likely due to spatial constraints within the simulations. Figures 13 and 14 show how spatially localized the high-speed streams can be. They also show that the observation of an earthward flow by the P3 satellite, in the simulations, is due to the spacecraft traversing a localized region with high speeds, as opposed to a feature that may be spatially broad but present for a short period of time. The high-speed stream is highly localized above and below the current sheet.

[24] During the time over which the two high-speed streams are observed by the actual P3 spacecraft, (0452–0500 UT) (Figure 9c) the satellite moved approximately 0.1 R$_E$, along its track. This is equivalent to 1.3 grid points within the simulation region. The scale size in each Cartesian direction is even smaller. If it is assumed that the actual satellite traversed a narrow channel of high-speed plasma, the simulation would not be able to resolve such a narrow feature, as a minimum of three grid points is needed to
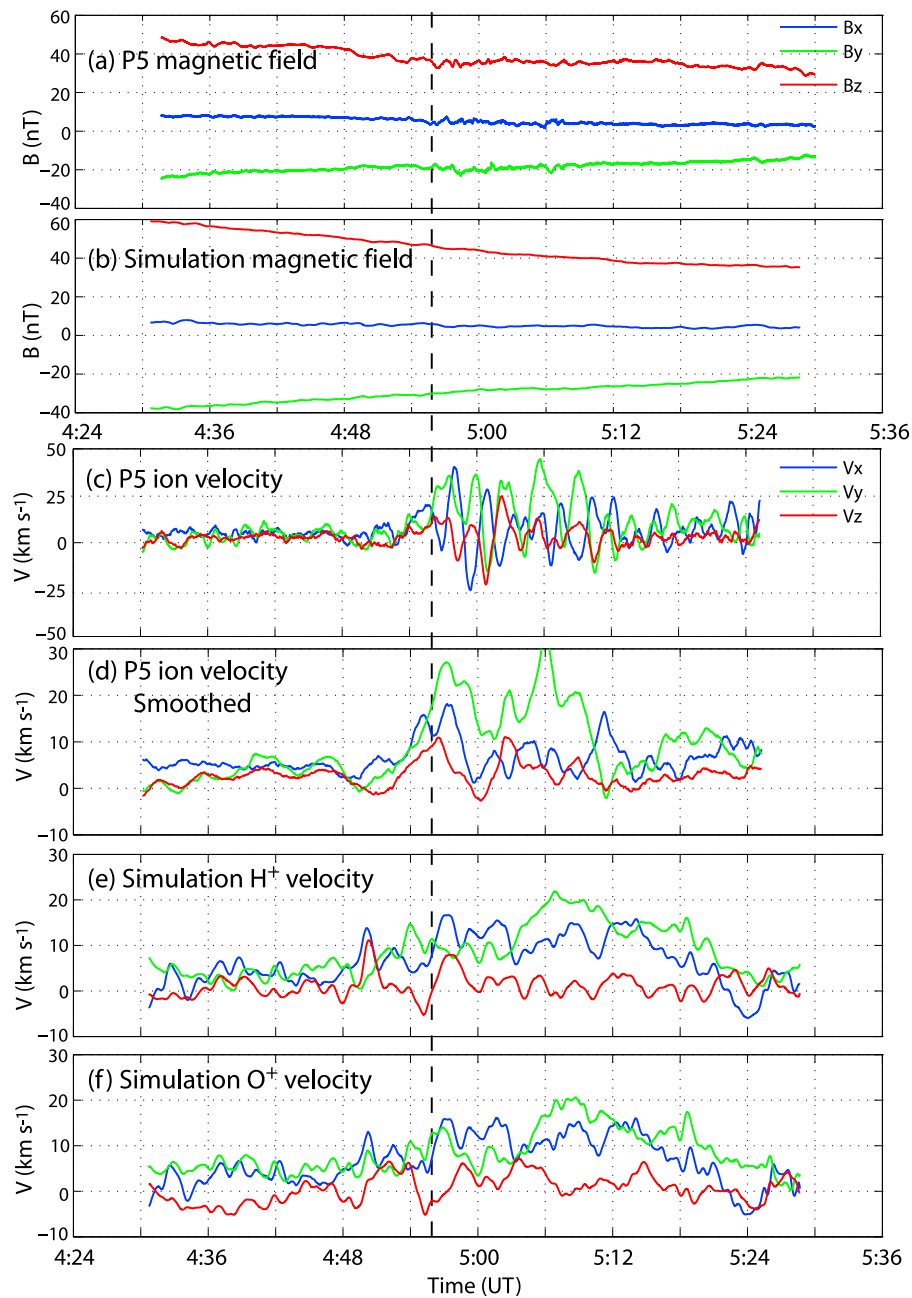
Figure 8. The same format as Figure 9 but for the P5 spacecraft. Like Figure 9, the spacecraft velocity data is both unsmoothed and smoothed. The smoothed data reduces the signatures of waves within the data. The dotted vertical line is the time identified by *Angelopoulos et al.* [2008] that the P5 satellite observed ion injection (~0456 UT).

resolve such a structure. In the simulation, the spatial extent of the high-speed region is approximately 0.37 R_E, or 5 grid points along track. And the feature is at least 2 grid points wide in each Cartesian direction.

[25] While the high-speed stream observed by the synthetic spacecraft appears to be more spatially broad than the one observed by the actual P3 spacecraft, the nature of the feature is very similar. The black and lavender dotted lines in Figure 9 indicate the beginning of observations of the high-speed stream for the actual and simulation spacecraft,

respectively. When the spacecraft velocity data is smoothed to account for the spatial limitations of the simulation (Figure 9d), the qualitative agreement with simulation results increases. The peak earthward velocity is within a factor of 2 (Figures 9d–9f) of the peak velocity seen in the simulation. For both actual and simulation results, entry into the high-speed stream is indicated not only by an increase in V_x, but also an increase in V_y. In both actual and simulation results the initial observation of duskward flows time lags the observation of earthward flows. The behavior of the
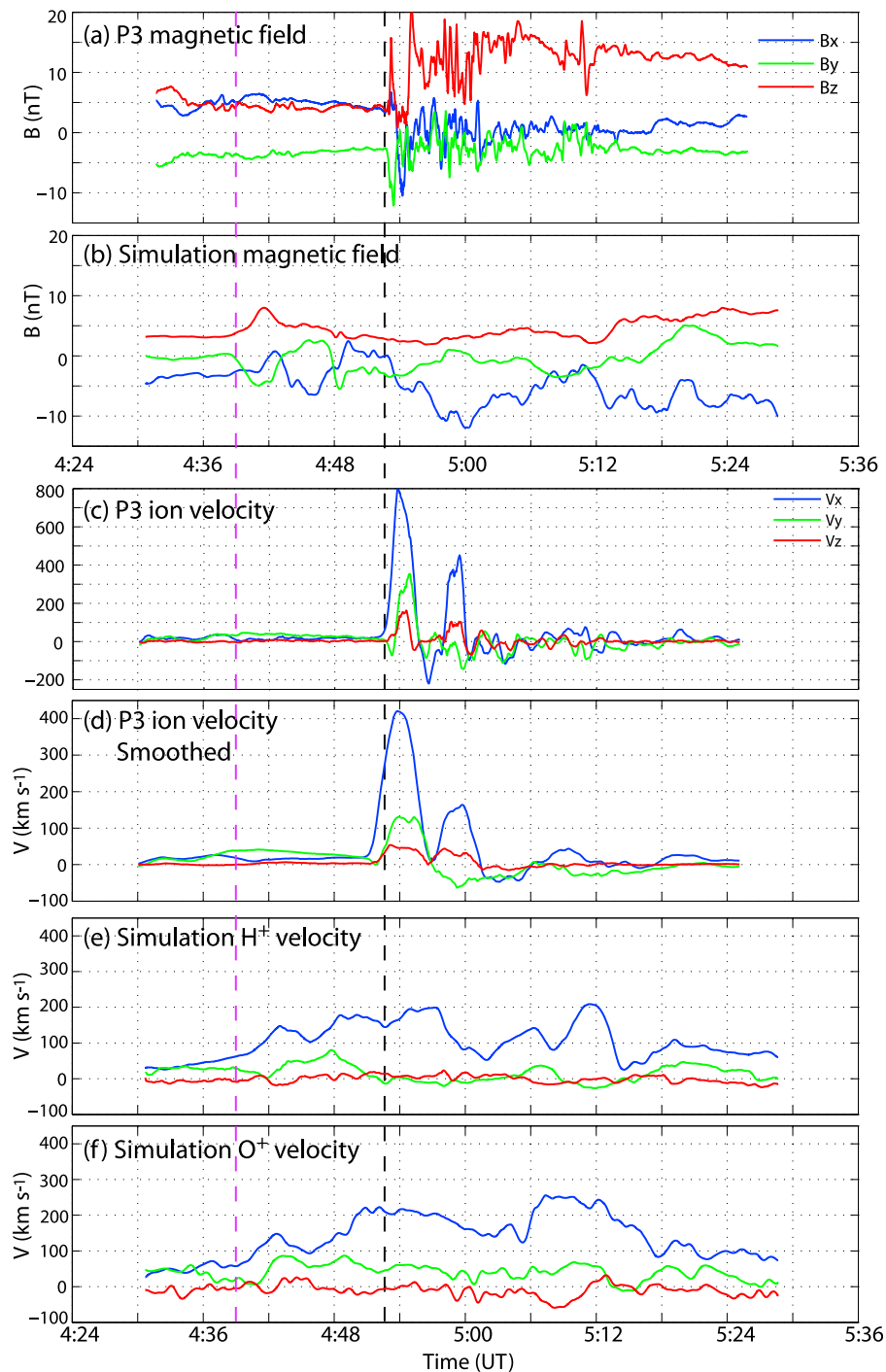
Figure 9. The same format as Figure 7 but for the P3 spacecraft. In addition to the values shown in Figure 7, Figure 9d shows the actual velocity data smoothed to partially account for spatial limitations in the model. The black dotted vertical line is the time identified by *Angelopoulos et al.* [2008] that the P3 satellite observed earthward flow onset (~0452:27 UT). The lavender dotted line (at ~0439 UT) is when the simulation P3 satellite first encounters the high-speed stream.

magnetic field components is also similar, with an increase in B_z upon entry into the stream, as well as a decrease in B_y, and first an increase then a decrease in B_x (Figures 9a–9b). This all implies that the simulation spacecraft observes a similar feature as the actual observations, it is just spread out over a larger spatial scale in the simulation leading to a broader time period over which the velocity increases and smaller peak values. When accounting for the spatial extent, the simulation spectrograms show a similar increase in energy and flux as the actual observations (Figure 10).
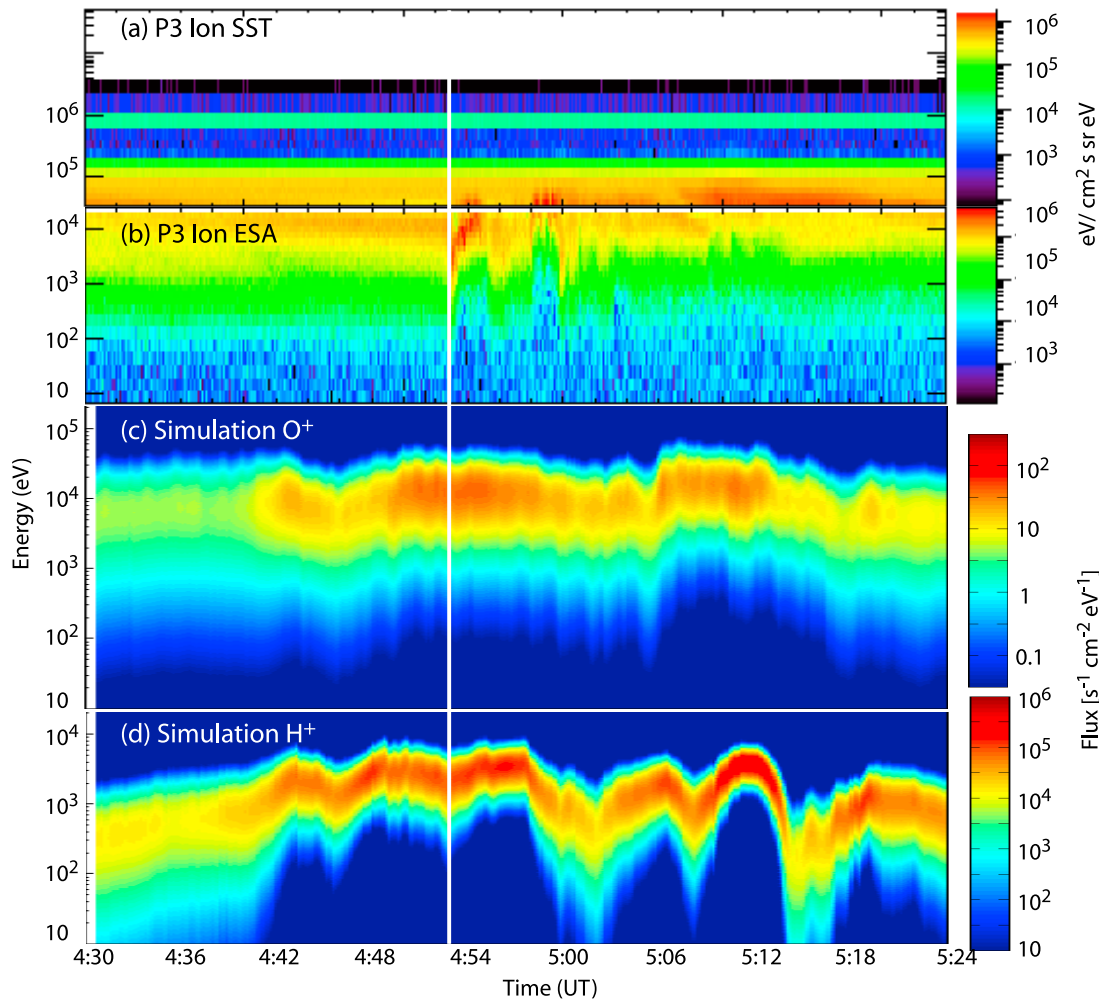
Figure 10. The same format as Figure 11 but for the P3 spacecraft. The white vertical line is at the same time as the dotted line in Figure 9.

[26] Entry of the P3 spacecraft into the high-speed stream is associated with a dipolarization. Figure 15 shows the total pressure in a plane parallel to the noon-midnight meridian but just earthward of the region in which the satellites are located. Prior to entry, the P3 spacecraft is in the plasmasphere (Figure 15a). Around 0440 UT dipolarization begins to occur (Figure 5e) and the local plasma sheet begins thinning (Figure 15b)). At approximately 0442 UT, the inner edge of the plasma sheet moves earthward, inside the location of the P3 spacecraft (Figure 15c) and P3 enters the plasma sheet, leading to the increase in energy and flux of ions (Figure 10).

[27] The simulation spacecraft at the P5 location observes the onset of dipolarization at the same time as the actual spacecraft. The magnitude of both the earthward and cross-tail components of the velocity for both hydrogen and oxygen increases (Figures 8e and 8f) at the same time as was actually observed (Figure 8c). The dipolarization is also evident in the oxygen spectrogram (Figure 12c), as an increase in energy but a decrease in flux. The magnitude of the magnetic field components is comparable for both actual and simulation spacecraft. After dipolarization, the actual magnetic field data (Figure 11a) shows evidence of high-frequency waves that the multifluid method does not resolve. (Figures 13 and 14)

3.3. Implications

[28] Prior to substorm onset, bright filaments were observed for several minutes in the auroral oval and were attributed to preconditioning of the magnetosphere [*Angelopoulos et al.*, 2008]. It is during this same time period that patchy reconnection is occurring in the tail in the simulation and a pseudo-breakup event is predicted. The occurrence of patchy reconnection prior to full cross-tail reconnection (Figures 4a–4c and Animation 1) suggests a reason for the previously reported spread of times between reconnection observations by a satellite and substorm onset.[1] Satellites may be observing a region of localized reconnection.

[29] The timing between the two events (reconnection versus onset) will be highly dependent on the location of the satellite(s) observing reconnection. Satellites may be observing patchy, localized reconnection occurring 10–15 min

_____
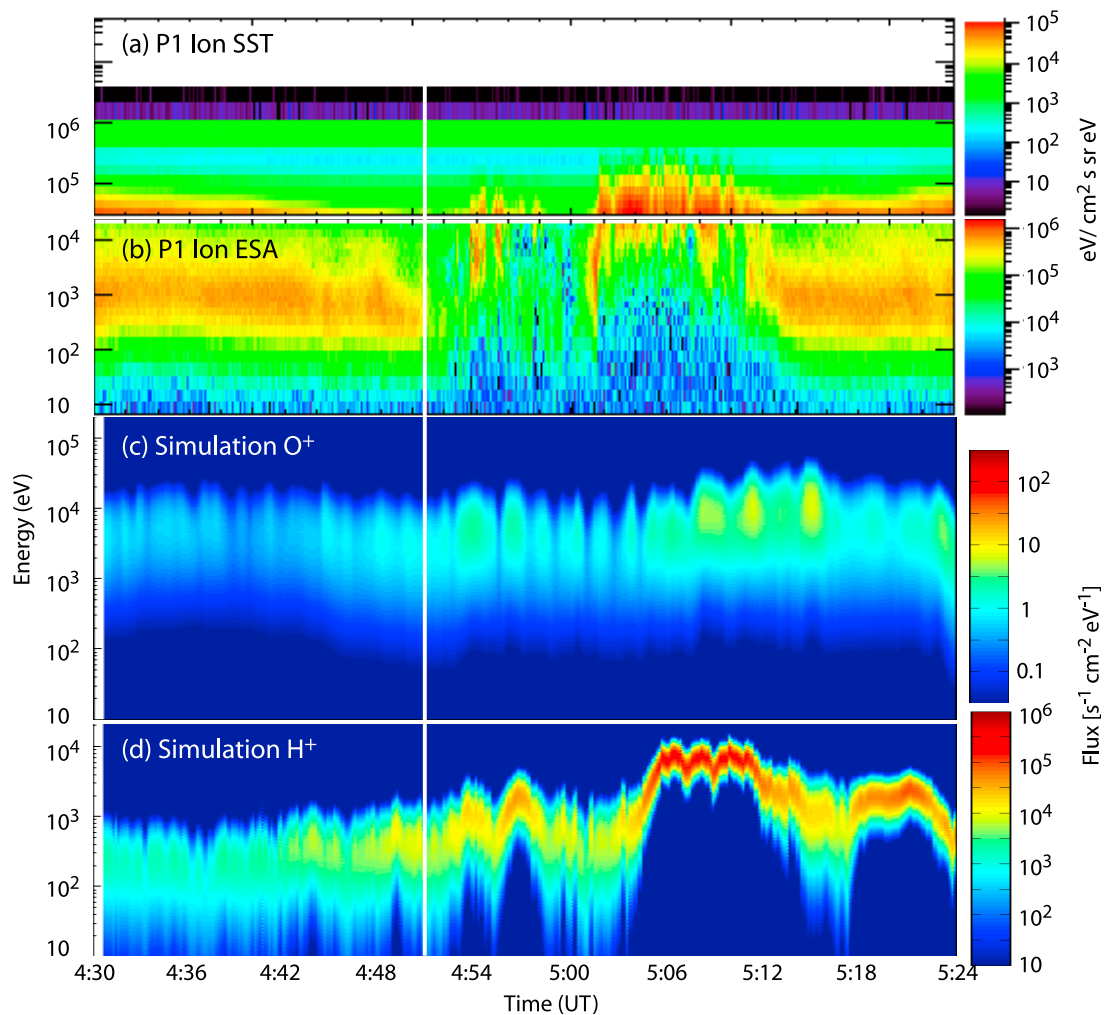[1]Animations are available in the HTML.

Figure 11. Ion spectrograms for the P1 satellite. (a) Data from the solid state telescope (SST) detector. (b) Data from the electrostatic analyzer (ESA) detector. (c and d) Spectrograms determined from the simulations for ionospheric O$^+$ and ionospheric H$^+$, respectively. The white vertical line is at the same time as the dotted line in Figure 7.

prior to full cross-tail reconnection. Or the satellite(s) may observe the full cross-tail reconnection, but not necessarily at the point of origin, thus inferring only a minute between reconnection and substorm onset. The simulations show that it takes on the order of 10 min for reconnection to propagate fully across the tail. These results indicate that depending on the location of the spacecraft, the timing between observed reconnection and substorm onset can vary from 1 to 20 min. In the case of the THEMIS satellites for this event, their trajectory was such that they were all below ecliptic plane, moving further away as time progressed, whereas the patchy reconnection initiated above the ecliptic plane (Figures 4a–4c). It was not until full cross-tail reconnection that the affects would have spread down to the satellite locations.

[30] The simulations also show that while reconnection is a necessary precursor for substorm onset, it is not sufficient. Patchy reconnection will lead to pseudo-breakup events. It is only after full cross-tail reconnection that substorm onset occurs and it is the result of plasma being injected into the

inner edge of the plasma sheet boundary (Figures 15c–15d). Expansion is associated with continued injection of plasma along the field lines into the poles (Figures 15e–15i). For the internally triggered substorm studied in this case, ionospheric outflows were the drivers of full cross-tail reconnection.

[31] These results (as well as those from the previous simulations for an idealized case [*Winglee et al.*, 2009]) indicate the reason for the continued controversy regarding the current disruption versus near-Earth neutral line models for substorm onset. The simulations agree with elements of both models. Figure 16 illustrates the timing of events. Y line reconnection occurs at ~20 R$_E$ (NENL model) but substorm onset is initiated by plasma injected into the inner edge of the plasma sheet (CD model). This can be seen as enhanced plasma pressures at ~10 R$_E$ (Figures 16a–16f). Figure 16c shows dipolarization occurring just prior to substorm onset. Continued injection of plasma leads to subsequent enhancement of the pressure at the inner edge of the plasma sheet (Figures 16e–16f) and equatorward expansion of the auroral
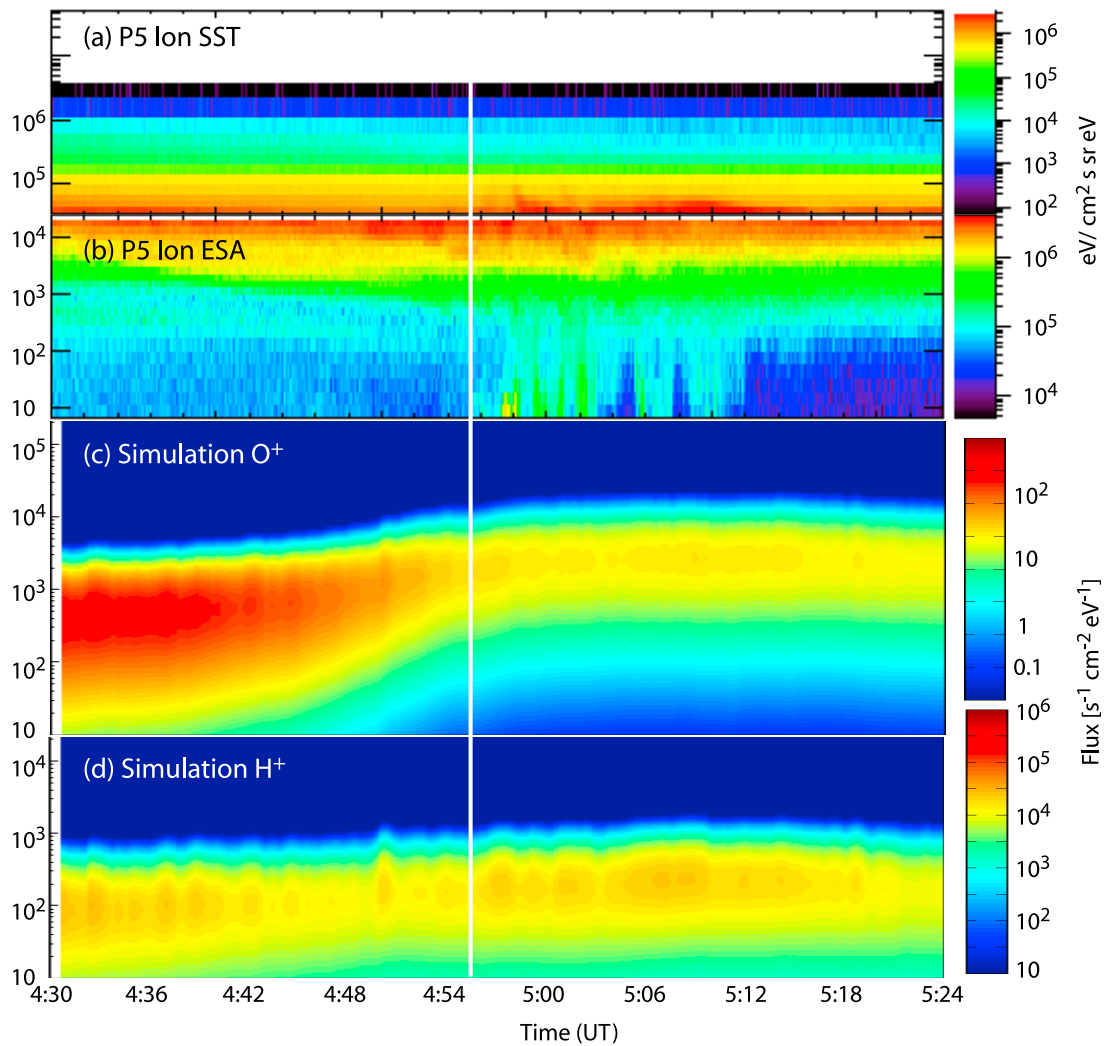
Figure 12. The same format as Figure 11 but for the P5 spacecraft. The white vertical line is at the same time as the dotted line in Figure 8.
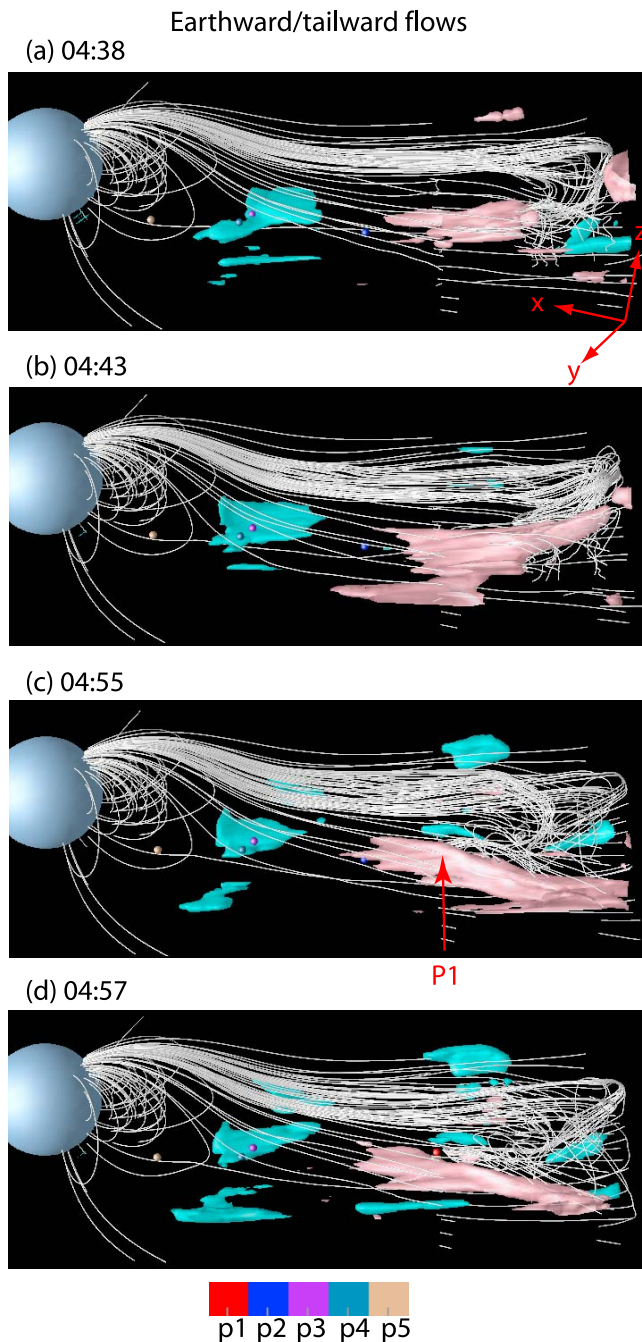
Earthward/tailward flows

Figure 13. The magnetic field and 3D surfaces of earthward (blue) and tailward (pink) flows of hydrogen as viewed from above the tail. The blue surfaces indicate regions with earthward speeds in excess of 100 km s^{-1}. The pink surfaces indicate regions with tailward speeds in excess of 250 km s^{-1}. The silver sphere is the inner boundary. The area shown is between -0.9 R$_E$ and -32.5 R$_E$ along x, ± 8.85 R$_E$ along y, and -6.5 R$_E$ and 3.5 R$_E$ along z. The instantaneous location of all five spacecraft are also indicated.

oval (Figures 16k–16l). Without reconnection at ~ 20 R$_E$ injecting plasma into the inner plasma sheet, the source of energy for the disruption of the inner edge of the plasma sheet at ~ 10 R$_E$ would not be present. Thus even though the processes leading to substorm onset occur at the inner edge

of the plasma sheet, they would not occur without prior reconnection further out in the tail.

4. Conclusions

[32] Simulations suggest the 0455 UT 26 February 2008 substorm was an internally triggered substorm and the process by which the substorm is initiated in the simulation is similar to that previously determined from an idealized case with purely southward IMF [*Winglee et al.*, 2009]. The sequence and timing of events determined for the idealized IMF case are that first an X line forms in the postplasmoid thin current sheet. This begins the growth phase of the substorm. Then Y line reconnection occurs within the thin current sheet, generating both earthward and tailward flux ropes. Earthward traveling flux ropes inject plasma into the plasmasphere when they dissipate at the inner edge of the plasma sheet. These injections can produce either pseudo-breakup events or substorm onset, depending on the size of the flux rope, and can occur on a ~ 1 min time scale. Ionospheric outflows play a key role in contributing to both substorm onset and breakup. This picture implies that elements of both the near-Earth neutral line (NENL) model and the current disruption (CD) model are correct. With regard to the observations for this specific event, the simulations agree with observations of reconnection prior to substorm onset (NENL model) [*Angelopoulos et al.*, 2008, 2009]. But the simulations also indicate that reconnection alone does not drive substorm onset. It is the result of plasma being injected into the inner edge of the plasma sheet (CD model) [*Lui et al.*, 2009].

[33] For the 0455 UT 26 February 2008 substorm, a thin current sheet forms after the ejection of a plasmoid. Within the postplasmoid current sheet, patchy reconnection occurs around 20 R$_E$ producing both small flux ropes and pseudo-breakup type current signatures in the polar cap. The southward IMF that drives the patchy reconnection also drives an ionospheric outflow with an enhanced concentration of oxygen ions. After approximately 10 min of patchy reconnection, the high concentration of heavy ions reaches the current sheet, increasing dissipation and energization of the plasma and initiating the full cross-tail reconnection at ~ 20 R$_E$, around local midnight. Plasma is injected into the inner magnetosphere, enhancing the plasma pressure at the inner edge of the plasma sheet, and initiating substorm onset. Continued injection leads to expansion.

[34] In analyzing the timing of both substorms that were observed by THEMIS on 26 February 2008, *Pu et al.* [2010] determined that a "two-step" scenario initiated both substorms, first an intensification of the aurora without expansion (i.e., a pseudo-breakup) and then large-scale oval brightening and expansion (substorm onset). For the 0455 UT storm, bright filaments were observed for several minutes prior to substorm onset [*Angelopoulos et al.*, 2008], possibly associated with a pseudo-breakup event. Substorm onset then occurred 1–2 min after reconnection was observed. The interpretation of the processes occurring prior to the onset of the 0455 UT substorm are qualitatively similar to those determined from simulations. The only variance is in the timing. While both the simulation satellites and the actual satellites see evidence of reconnection at the same time, the global nature of the simulations and local nature of satellite
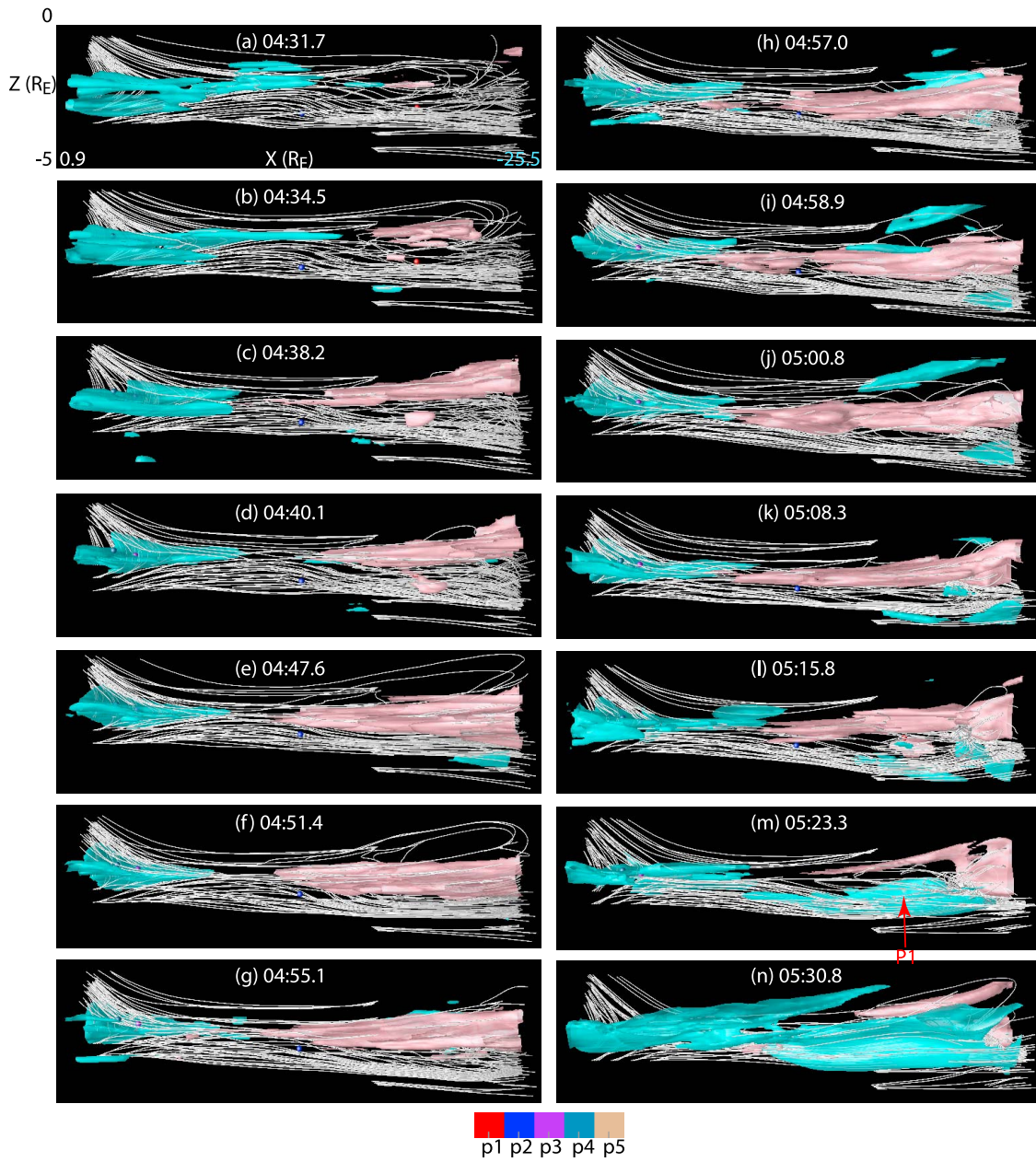
Figure 14. The magnetic field and 3D surfaces of earthward (blue) and tailward (pink) flows of hydrogen, now, as viewed from dusk. The surfaces are at the same values as in Figure 13 but the area shown is just the reconnection region. As the area is a subset of the region in Figure 13 only spacecraft P1–P4 are visible.
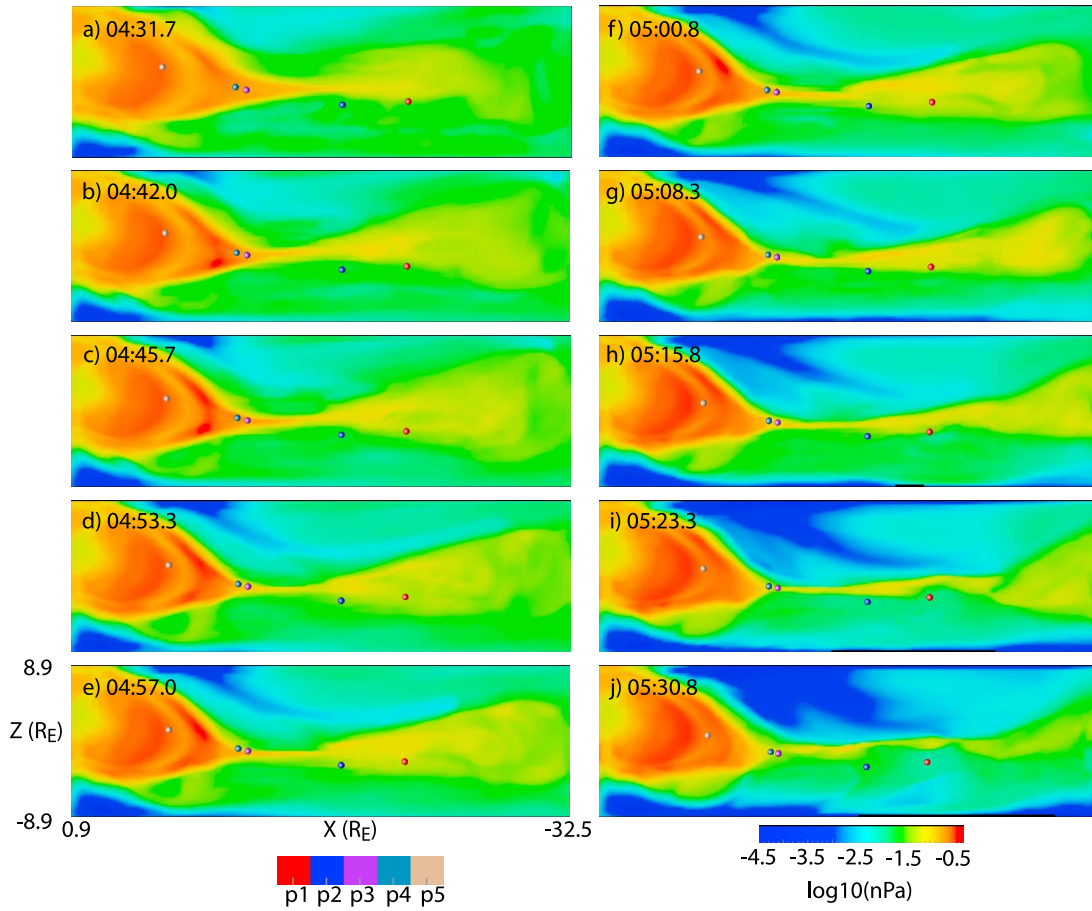
HARNETT ET AL.: SUBSTORM SIMULATION

Figure 15. The total plasma pressure in a plane parallel to the noon-midnight meridian but just earthward of the plane that the spacecraft are in. The location of the spacecraft are also indicated at each time.
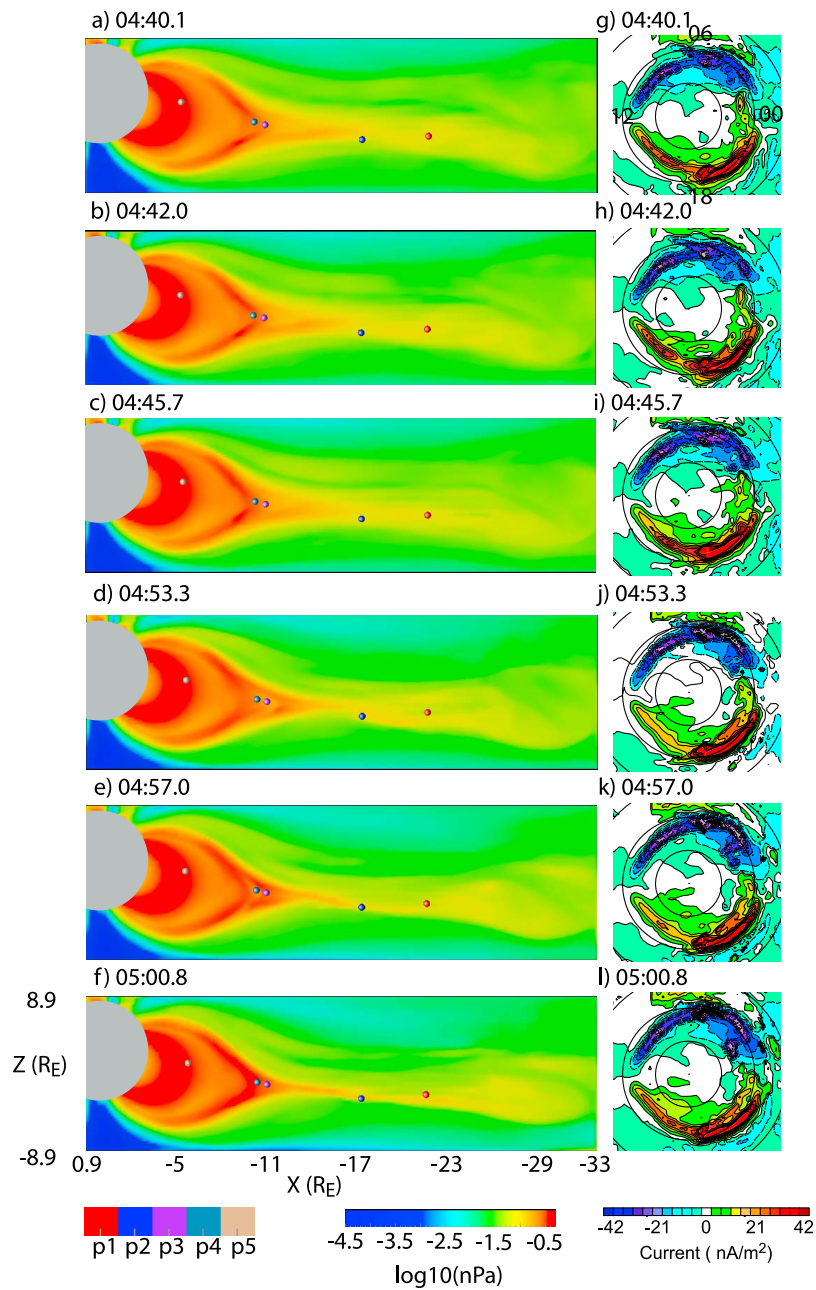
Figure 16. The total plasma pressure in (left column) the noon-midnight meridian and (right column) the current in the polar cap. The silver circle in the pressure plots indicates the inner boundary. The current plots the same format as those in Figure 3 but are zoomed in and rotated counterclockwise 90° in order to highlight the equatorward expansion (to the right). The inner most latitude circle is 80° MLT, with the next further out 70°. The location of the spacecraft are also indicated at each time in the pressure plots.

observations leads to a difference in classifying when reconnection occurred, with the simulations indicating it was initiated approximately 20 min earlier than the satellite observations. This highlights the difficulty in using local satellite observations for timing substorm onset.

References

Angelopoulos, V., et al. (2008), Tail reconnection triggering substorm onset, *Science*, *321*, 931, doi:10.1126/science.1160495.

Angelopoulos, V., et al. (2009), Response to comment on Tail Reconnection Triggering Substorm Onset, *Science*, *324*, 1391-c, doi:10.1126/science.1168045.

Baker, D. N., et al. (1996), Neutral line model of substorms: Past results and present view, *J. Geophys. Res.*, *101*, 12,975–13,010.

Baker, D. N., et al. (2002) Timing of magnetic reconnection initiation during a global magnetospheric substorm onset, *Geophys. Res. Lett.*, *29*(24), 2190, doi:10.1029/2002GL015539.

Hones, E. W., Jr. (1984), Plasma sheet behavior during substorms, in *Magnetospheric Reconnection in Space and Lab Plasmas*, *Geophys.* *Monogr. Ser.*, vol. 30, edited by E. W. Hones Jr., p. 178, AGU, Washington, D. C.

Lui, A. T. Y. (1996), Current disruption in the Earth's magnetosphere: Observations and models, *J. Geophys. Res.*, *101*, 13,067–13,088.

Lui, A. T. Y., et al. (1992), Current disruptions in the near-Earth neutral sheet region, *J. Geophys. Res.*, *97*, 1461–1480.

Lui, A.T.Y., et al. (2009), Comment on Tail Reconnection Triggering Substorm Onset, *Science*, *325*, 1391-b, doi:10.1126/science.1167726.

Meng, C.-I. and K. Liou (2004), Substorm timings and timescales: A new aspect, *Space Sci. Rev.*, *113*, 41–75, doi:10.1023/B:SPAC.0000042939.88548.68.

Pu, Z. Y., et al. (2010), THEMIS observations of substorms on 26 February 2008 initiated by magnetotail reconnection, *J. Geophys. Res.*, *115*, A02212, doi:10.1029/2009JA014217.

Slavin, J. A., et al. (2003), Cluster four spacecraft measurements of small traveling compression regions in the near-tail, *Geophys. Res. Lett.*, *30*(23), 2208, doi:10.1029/2003GL018438.

Winglee, R. M. (2004), Ion cyclotron and heavy ion effects on reconnection in a global magnetotail, *J. Geophys. Res.*, *109*, A09206, doi:10.1029/2004JA010385.

Winglee, R. M., E. Harnett, and A. Kidder (2009), Relative timing of substorm processes as derived from multifluid/multiscale simulations: Internally driven substorms, *J. Geophys. Res.*, *114*, A09213, doi:10.1029/2008JA013750.

E. M. Harnett, T. Lerud, and R. M. Winglee, Department of Earth and Space Sciences, Box 351310, University of Washington, Seattle, WA 98195-1310, USA. (eharnett@ess.washington.edu; cpaty@u.washington.edu; winglee@ess.washington.edu)